ISSN 2447-6102

Article

Numerical analysis of wave propagation and vibration of overhead transmission cable

Silva, G.[1,] *, Machado, M.R.[1], Dutkiewicz, M.[2], and Dos Santos, J.M.C[3]

[1] Department of Mechanical Engineering, University of Brasilia, 70910-900, Brasilia, Brazil; gabrielcs.eng@gmail.com; marcelam@unb.br

[2] Faculty of Civil, Environmental Engineering and Architecture, University of Science and Technology, 85-796 Bydgoszcz, Poland; macdut@utp.edu.pl

[3] University of Campinas, UNICAMP-FEM-DMC, Rua Mendeleyev 200, Cidade Universitária Zeferino Vaz, Campinas, SP, Brazil; zema@fem.unicamp.br

* Correspondence: gabrielcs.eng@gmail.com;

Received: 17/08/2020; Accepted: 25/08/2020; Published: 02/09/2020

Abstract: This paper presents a comparison of numerical methods used to model and analyse the vibration of overhead transmission line conductor. The cable vibration signature is expressed through the frequency response function (FRF) and the flexural wave propagation via dispersion diagram. The cable is modelled under the numerical background of the finite element, spectral element, spectral transfer matrix, and wave finite element methods. Efficacy, accuracy and computational effort to estimate the FRF and dispersion diagram results demonstrate the advantage and limitation of each technique. It is recommended to analyse the vibrations of the systems in different configurations of initial and boundary conditions because some initial condition likewise tensile force, changes the dynamic response and the type of waves. The numerical analysis investigates the natural frequency, mode shape and flexural waves estimated from the four methods for different tensile force and boundary condition.

Keywords: Overhead transmission cable; Flexural wave propagation; Wave Finite Element; Spectral transfer matrix; Spectral element method.

1. Introduction

Overhead transmission conductor cables are long and slender structures responsible for the transmission of electrical energy over long distances (Fu and Li, 2016). Due to the high demand for electrical energy, the transmission system must be reliable and resistant to vibrations induced by the wind, temperature variations, static loads, corrosion and wire fatigue (Li et al., 2018). Local and global failures are known as the cascade effect, it happens when a failure spread its effect to the whole transmission line like as, towers, cables and to the neighbouring towers. Excessive vibration is one of the common causes of damages and fatigues in cables, therefore the importance of characterising the dynamic response of this system.

The analytical solution of the Euler-Bernoulli beam subjected to an axial load and the natural frequency and mode shape formulation for a simple supported cable as described by Rao (2018) are reviewed. Transmission line conductor cable is a complex structure composed of multi-wire that must be considered in the numerical analysis. Therefore, the requirement for effective and practical tools to model conductor cables, since an analytical solution does not exist. The common numerical technique is the Finite Element Method (FEM) (Zienkiewicz, 2000). Researchers have also been used the Spectral Element Method (SEM) (Doyle, 1997; Lee, 2004) and the Wave Finite Element (WFE) method to simulate the dynamic behaviour of the cables. Proposed by Lee (2000, 2004) the Spectral Transfer Matrix (STM) method uses the spectral element matrix computed directly from the transfer (or transition) matrix formulated

from the state-space equation of motion of a structure. The STM can be efficiently used to model periodic structures and to estimate the dispersion diagram.

Schaal et al. (2015) presented the propagation of waves in coupled multi-wire cables using experimental tests and numerical methods (FEM and WFE). Based on these numerical and experimental results they showed a strong dependence of the coupling characteristics. Bischoff et al. (2015) presented an analysis of wave propagation in periodic 3D waveguides based on WFE. Machado et al. (2020) developed a spectral element for the transmission conductor cable, including the hysteretic and aerodynamic damping effect using the SEM. The efficiency of SEM to calculate the dynamic cable response has been explored in Dutkiewicz and Machado (2019a, 2019b, 2019c, 2019d). The results of the SEM showed very good precision as compared to the experimental measurements.

The main objective of this paper is to verify the dynamic behaviour and the flexural wave propagation of the overhead transmission conductor cable modelled by SEM, STM, FEM, and WFE. Compare the accuracy and efficiency between these numerical techniques. Simulated examples are performed and the results demonstrated the efficiency and the particularity of each numerical tool, besides checking the computational cost and accuracy.

2. Cable structural element analytical solution

The analytical solution of vibrations in a beam is treated in Rao (2018) and is extended here including the tensile load action to model a cable. Figure 1 shows a slender flexural beam under tensile load and a typical infinitesimal element. By considering the free-body diagram represented in Figure 1(b), the external forces per unit length are the bending moment, *M*(*x*,*t*), shear force *V* (*x*, *t*), and axial or tensile load *T* (*x, t*). Therefore, it must consider the effects of other external forces *f(x,t)* (Figure 1a), that induces lateral vibrations.

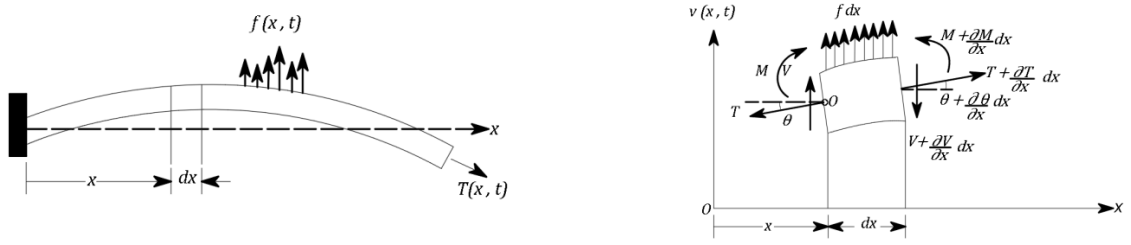

(a) (b)

Figure 1. Slender flexural beam: (a) external and tensile loads; (b) infinitesimal beam element (Rao,2018).

Applying the dynamic equilibrium equation, the vertical motion is obtained as:

$$-(V+dV)+fdx+V+(T+dT)\sin(\theta+d\theta)-T\sin\theta=\rho A\,dx\frac{\partial^2 v}{\partial t^2}, \tag{1}$$

where $dV=\partial V/\partial x\,dx$, A is the cross-section area, ρ the material mass density, v and θ are the vertical and the rotational displacements, respectively. The motion equation around the point *O* is obtained as:

$$(M+dM)-(V+dV)dx+fdx\frac{dx}{2}-M=0, \tag{2}$$

where $dM=\partial M/\partial x\,dx$. By using the relationship $V=\partial M/\partial x\,dx$ and from the Euler-Bernoulli thin beam theory, the relationship between bending moment and deflection can be expressed as:

$$M=EI\frac{\partial^2 v}{\partial x^2}. \tag{3}$$

where *E* is the elastic modulus and *I* is the inertia moment. Assuming small displacement and combining Eq. (1) and (2) the cable differential equation of motion is obtained as:

$$\frac{\partial^2}{\partial x^2}\left[EI\frac{\partial^2 v}{\partial x^2}\right]+\rho A\frac{\partial^2 v}{\partial t^2}-T\frac{\partial^2 v}{\partial x^2}=f(x,t), \tag{4}$$

or in the homogeneous form as:

$$EI\frac{\partial^4 v(x,t)}{\partial x^4}-T\frac{\partial^2 v(x,t)}{\partial x^2}+\rho A\frac{\partial^2 v(x,t)}{\partial t^2}=0. \tag{5}$$

The solution of Eq. (5) can be obtained via separation of variables technique. Assuming harmonic solution $v(x,t) = \mathrm{v}(x)(A\ cos\ \omega t\ +\ B\ sin\ \omega t)$, where $\mathrm{v}(x) = C^{sx}$. For a simply supported beam under axial force, the natural frequency can be written as:

$$\omega_n = \frac{\pi^2}{L^2}\sqrt{\frac{EI}{\rho A}}\left(n^4 + \frac{n^2 T L^2}{\pi^2 EI}\right)^{\frac{1}{2}}, \quad n = 1,2,\ldots. \tag{6}$$

where ρA is mass per unit length, EI is the uniform bending rigidity, L is the cable length, T is tension force, and $v(x,t)$ is the cable displacement as a function of the position x and time t.

3. Numerical techniques to model the cable

The conductor cable is modelled by FEM, WFE, SEM, and STM methods. Each technique incorporates its own particularity and applicability. The forced response are calculated by SEM, FEM and WFE, while the dispersion diagram are obtained by SEM, WFE and STM. These methods are brefily reviewed here, for more details see the references.

3.1. Finite element method

The FEM is a mesh technique used to simulate the physical phenomenon of structures and general systems. It is a discretization method, as illustrated in Figure 2. The elements are formulated based on partial differential equations which are solved in an approximate way, by discretizing the domain with elements and nodes.

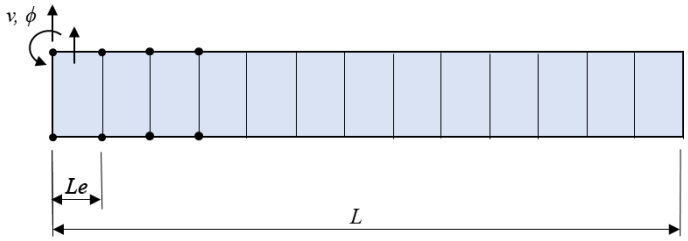

Figure 2. Finite element mesh discretisation.

By multiplying the equation of motion by a test function and integrating it over a sub-domain of the system leads to

$$\int_{x_e}^{x_e+1}\left(EI\frac{\partial^4 v}{\partial x^4} - T\frac{\partial^2 v}{\partial x^2} + \rho A\frac{\partial^2 v(x,t)}{\partial t^2}\right)dx = 0\,. \tag{7}$$

Considering a constant coefficient a displacement solution as:

$$v(x,t) = \boldsymbol{N}(x)\boldsymbol{v}(t)\,, \tag{8}$$

where $\boldsymbol{N}$ is the shape function matrix. Substituting the Eq.(8) in (7) it has:

$$\int_{x_e}^{x_e+1}\left(-EI\frac{\partial^2 \boldsymbol{N}^T}{\partial x^2}\frac{\partial^2 \boldsymbol{N}}{\partial x^2}\boldsymbol{v} - T\frac{\partial \boldsymbol{N}^T}{\partial x}\frac{\partial \boldsymbol{N}}{\partial x}\boldsymbol{v} + \rho A\boldsymbol{N}^T\boldsymbol{N}\ddot{\boldsymbol{v}}\right)dx = 0\,, \tag{9}$$

where the stiffness matrix of an element of length l is given by,

$$\boldsymbol{K_e} = \int_0^l\left(-\boldsymbol{EI}\frac{\boldsymbol{\partial^2 N^T}}{\boldsymbol{\partial x^2}}\frac{\boldsymbol{\partial^2 N}}{\boldsymbol{\partial x^2}}\boldsymbol{v} - \boldsymbol{T}\frac{\boldsymbol{\partial N^T}}{\boldsymbol{\partial x}}\frac{\boldsymbol{\partial N}}{\boldsymbol{\partial x}}\boldsymbol{v}\right)\boldsymbol{dx}$$

$$= \frac{\boldsymbol{EI}}{\boldsymbol{l^3}}\begin{bmatrix} \boldsymbol{12} & \boldsymbol{6l} & \boldsymbol{-12} & \boldsymbol{6l} \\ \boldsymbol{6l} & \boldsymbol{4l^2} & \boldsymbol{-6l} & \boldsymbol{2l^2} \\ \boldsymbol{-12} & \boldsymbol{-6l} & \boldsymbol{12} & \boldsymbol{-6l} \\ \boldsymbol{6l} & \boldsymbol{2l^2} & \boldsymbol{-6l} & \boldsymbol{4l^2} \end{bmatrix} + \frac{\boldsymbol{T}}{\boldsymbol{10\,l}}\begin{bmatrix} \boldsymbol{12} & \boldsymbol{l} & \boldsymbol{-12} & \boldsymbol{l} \\ \boldsymbol{l} & \boldsymbol{(4/3)l^2} & \boldsymbol{-l} & \boldsymbol{-l^2/3} \\ \boldsymbol{-12} & \boldsymbol{-l} & \boldsymbol{12} & \boldsymbol{-l} \\ \boldsymbol{l} & \boldsymbol{-l^2/3} & \boldsymbol{-l} & \boldsymbol{(4/3)l^2} \end{bmatrix} \tag{10}$$

and the corresponding mass matrix is,

$$\boldsymbol{M_e} = \int_0^l \boldsymbol{\rho A N^T N}\, \boldsymbol{dx} = \frac{\boldsymbol{\rho A l}}{\boldsymbol{420}} \begin{bmatrix} \boldsymbol{156} & \boldsymbol{22l} & \boldsymbol{54} & \boldsymbol{-13l} \\ \boldsymbol{22l} & \boldsymbol{4l^2} & \boldsymbol{13l} & \boldsymbol{-3l^2} \\ \boldsymbol{54} & \boldsymbol{13l} & \boldsymbol{156} & \boldsymbol{-22l} \\ \boldsymbol{-13l} & \boldsymbol{-3l^2} & \boldsymbol{-22l} & \boldsymbol{4l^2} \end{bmatrix} \tag{11}$$

Including the external forces, the Eq. (9) can be rewritten in matrix form as,

$$\boldsymbol{M_e \ddot{v}} + \boldsymbol{K_e v} = \boldsymbol{f_e}. \tag{12}$$

By rewriting the Eq.(12) in the frequency domain it has,

$$(-\omega^2 \boldsymbol{M_e} + \boldsymbol{K_e})\, \hat{\boldsymbol{v}} = \hat{\boldsymbol{f}}_e. \tag{13}$$

3.2. Wave finite element metod

By considering a homogeneous cable as a set of small cross section slices, or cable unit-cells (Fig. 3), it can be seen as a periodic structure (Fig. 3). WFE is a wave propagation periodic solution based on the FEM, which allows us to solve the wave propagation and vibration problems by analyzing only one period (or one cell) of the structure (Mencik and Ichchou, 2005; Mencik,2008; Mace and Manconi, 2008, 2005; Duhamel, 2006). The equilibrium equation for the FEM element can be written in terms of its dynamic stiffness matrix as $\boldsymbol{D_e} = -\omega^2 \boldsymbol{M_e} + \boldsymbol{K_e}$ (Eq. 13). For a periodic structure the WFE (Fig. 3) unit-cell can be formulated based on the FEM element stiffness and mass matrices expressed in the Eq.(12) and (13).

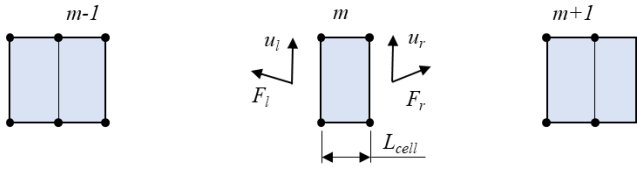

Figure 3. A cell *m* of a cylindrical waveguide with displacement fields and forces on the left and right cross-section.

The unit-cell dynamic stiffness matrix can be partitioned in left-side (l) and right-side (r) degrees-of-freedom (DOF), and the motion equation can be written as:

$$\begin{bmatrix} \boldsymbol{D_{ll}} & \boldsymbol{D_{lr}} \\ \boldsymbol{D_{rl}} & \boldsymbol{D_{rr}} \end{bmatrix} \begin{Bmatrix} \boldsymbol{u_l} \\ \boldsymbol{u_r} \end{Bmatrix} = \begin{Bmatrix} \boldsymbol{F_l} \\ \boldsymbol{F_r} \end{Bmatrix}, \tag{14}$$

where $\boldsymbol{u_n}$ are the displacement fields and $\boldsymbol{F_n}$ are the force vectors with $n = l, r$. If required the internal DOFs can also be included in the dynamic stiffness matrix (Nobrega at al., 2016). Rearranging the eq.(14) as a Transfer Matrix formulation one produces,

$$\begin{Bmatrix} \boldsymbol{u_r} \\ \boldsymbol{-F_r} \end{Bmatrix} = \begin{bmatrix} \boldsymbol{-D_{lr}^{-1} D_{ll}} & \boldsymbol{-D_{lr}^{-1}} \\ \boldsymbol{D_{rl} - D_{rr} D_{lr}^{-1} D_{ll}} & \boldsymbol{-D_{rr} D_{lr}^{-1}} \end{bmatrix} \begin{Bmatrix} \boldsymbol{u_l} \\ \boldsymbol{F_l} \end{Bmatrix} \quad \text{or} \quad \mathbf{q_r} = \mathbf{T q_l}, \tag{15}$$

where $\boldsymbol{T}$ is the transfer matrix that relates the left state vector $\boldsymbol{q_l}$ with the right state vector $\boldsymbol{q_r}$ of the unit-cell. Since $\boldsymbol{T}$ depends on $\boldsymbol{D_{lr}^{-1}}$, for some cases it could be ill-conditioned. Not shown here, to avoid it a formulation using the state vector by displacement alone can be applied (Zhong, 1995).

Consider now consecutive unit-cells, *m* and *m+1* (Fig. 3), the displacement continuity condition is $\boldsymbol{u_r}^{(m)} = \boldsymbol{u_l}^{(m+1)}$ and the force balance $\boldsymbol{F_r}^{(m)} = -\boldsymbol{F_l}^{(m+1)}$, which produces $\boldsymbol{q_r}^{(m)} = \boldsymbol{q_l}^{(m+1)}$. Substituting in the Eq.(15), produces:

$$\mathbf{q_l}^{(\boldsymbol{m+1})} = \mathbf{T q_l^{(m)}}. \tag{16}$$

Applying the Floquet-Bloch's theorem for an infinite periodic system (Mead, 1973) applied to consecutive unit-cells, generates $\boldsymbol{u_l^{(m+1)}} = e^{\mu}\, \boldsymbol{u_l^{(m)}}$ and $\boldsymbol{F_l^{(m+1)}} = -e^{\mu}\, \boldsymbol{F_l^{(m)}}$, where $\mu = -i\beta L_{cell}$ is the attenuation constant, and β is the Bloch wavenumber (Xiao, 2012). Substituting displacement and force vectors in Eq. (16), rearranging and disregarding the subscript l and superscript *m* it produces,

$$\mathbf{T}\begin{Bmatrix}\boldsymbol{u}_l^{(m)}\\ \boldsymbol{F}_l^{(m)}\end{Bmatrix} = \boldsymbol{e}^{\boldsymbol{\mu}}\begin{Bmatrix}\boldsymbol{u}_l^{(m)}\\ \boldsymbol{F}_l^{(m)}\end{Bmatrix} \quad \text{or} \quad \mathbf{Tq} = \boldsymbol{e}^{\boldsymbol{\mu}}\mathbf{q}, \tag{17}$$

which is the Bloch wave eigenproblem where e^{μ} are the eigenvalues and $\boldsymbol{q}$ are the corresponding eigenvectors. Therefore the *2n* eigenvalues, when ordered appropriately, can be subdivided into two groups: $|e^{\mu_j}| \leq 1, j = 1,2,\dots,n$, which corresponds to the waves travelling to the right and $|e^{-\mu_j}| \geq 1, j = 1,2,\dots,n$ which corresponds to waves travelling to the left. Then, the state vectors $\boldsymbol{q}^{(m)}$ for a finite structure can be expressed as (Silva, 2014):

$$\mathbf{q}^{(m)} = \sum_{\boldsymbol{j}} \boldsymbol{\Phi_j}\, \mathbf{Q}_{\boldsymbol{j}}^{(\boldsymbol{m+1})} = \sum_{\boldsymbol{j}} \boldsymbol{\Phi_j}\, \boldsymbol{e}^{-\boldsymbol{i\beta_j L_{cell}}}\mathbf{Q}_{\boldsymbol{j}}^{\boldsymbol{m}}, \quad \text{with} \quad \boldsymbol{m} = \mathbf{1},\mathbf{2},\mathbf{3},\dots,\boldsymbol{N_c},\boldsymbol{N_{c+1}}, \tag{18}$$

where N_c is the number of cells, β_j is the Bloch wavenumber, Φ_j is the eigenvector or wavemode, and $\boldsymbol{Q}_j^{(m+1)}$ and $\boldsymbol{Q}_j^{(m)}$ are the wave vector amplitudes at the unit-cell boundary conditions $m+1$ and m, respectively.

3.3. Spectral element method

The undamped Euler-Bernoulli beam equation of motion subjected to axial force and under bending vibration is governing by the Eq. (1). Figure 4 shows an elastic two-node element with a uniform rectangular cross-section subjected to an axial force. Internal structural damping is introduced by a complex Young´s modulus, $E = E(1 + i\eta)$ where η is the hysteretic structural loss factor and $i = \sqrt{-1}$.

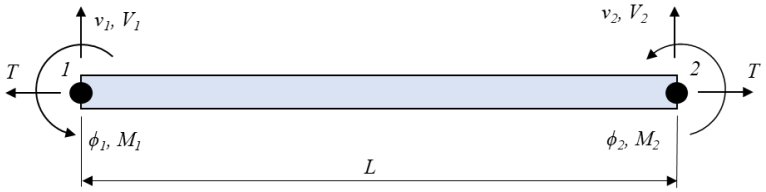

Figure 4. Two-node spectral element

By considering a constant coefficient, the vertical displacement solution can be assumed of the form:

$$v(x,t) = v_0 e^{-i(kx-\omega t)}, \tag{19}$$

where v_0 is the amplitude, ω is the circular frequency and k is the wavenumber. Substituting Eq.(19) in the Eq. (5), the dispersion equation is obtained as,

$$k^4 + \alpha k^2 - k_F^4 = 0, \tag{20}$$

where $\alpha = T/EI$ and $k_F = \sqrt{\omega}(\rho A/EI)^{1/4}$ is the wavenumber for the flexural wavemode. By solving the Eq.(20) four wavenumbers are obtained which can be written as:

$$k_{1,3} = \pm\sqrt{\left[\left(\frac{\alpha}{2}\right)^2 + k_F^4\right]^{1/2} - \frac{\alpha}{2}}, \text{ and } k_{2,4} = \pm i\sqrt{\left[\left(\frac{\alpha}{2}\right)^2 + k_F^4\right]^{1/2} + \frac{\alpha}{2}}. \tag{21}$$

Substituting Eq. (21) in (19) the general solution for the beam spectral element of length L subjected to an axial load, it can be expressed as,

$$v(x,\omega) = a_1 e^{-ik_1 x} + a_2 e^{-k_2 x} + a_3 e^{-ik_1(L-x)} + a_4 e^{-k_2(L-x)} = \boldsymbol{s}(x,\omega)\boldsymbol{a} \tag{22}$$

where $\boldsymbol{s}(x,\omega) = \left\{e^{-ik_1 x}, e^{-k_2 x}, e^{-ik_1(L-x)}, e^{-k_2(L-x)}\right\}$ and $\boldsymbol{a}(x,\omega) = \{a_1, a_2, a_3, a_4\}^T$. The spectral nodal displacements and slopes of the beam element are related to the displacement field at node 1 $(x = 0)$ and node 2 $(x = L)$, by

$$\mathbf{d} = \begin{bmatrix} v_1 \\ \phi_2 \\ v_2 \\ \phi_2 \end{bmatrix} = \begin{bmatrix} v(0) \\ v'(0) \\ v(L) \\ v'(L) \end{bmatrix} = \begin{bmatrix} s(0,\omega) \\ s'(0,\omega) \\ s(L,\omega) \\ s'(L,\omega) \end{bmatrix} \boldsymbol{a} = \boldsymbol{G}(\omega)\boldsymbol{a} \tag{23}$$

where

$$\boldsymbol{G}(\omega) = \begin{bmatrix} 1 & 1 & e^{-ik_1 L} & e^{-k_2 L} \\ -ik_1 & -k_2 & ik_1 e^{-ik_1 L} & k_2 e^{-k_2 L} \\ e^{-ik_1 L} & e^{-k_2 L} & 1 & 1 \\ -ik_1 e^{-ik_1 L} & -k_2 e^{-k_2 L} & ik_1 & k_2 \end{bmatrix} \tag{26}$$

The frequency-dependent displacement within an element is interpolated from the nodal displacement vector $\mathbf{d}$, by eliminating the constant vector $\boldsymbol{a}$ from Eq. (23) and by using Eq. (25) it is expressed as $v(x,\omega) = \mathbf{g}(x,\omega)\mathbf{d}$. where the shape function is $\mathbf{g}(x,\omega) = \boldsymbol{s}(x,\omega)\boldsymbol{G}^{-1}(\omega)$. The dynamic stiffness matrix for the spectral beam element under axial tension can be obtained by:

$$\boldsymbol{S}(\omega) = EI \left[\int_0^L \mathbf{g}''(x)^T \mathbf{g}''(x) dx - k^4 \int_0^L \mathbf{g}(x)^T \mathbf{g}(x) dx \right] + T \int_0^L \mathbf{g}'(x)^T \mathbf{g}'(x) dx \tag{27}$$

where (') expresses the space partial derivative. Calculating the integrals in Eq. (27) the dynamic stiffness matrix is obtained. For the sake of conciseness matrix $\boldsymbol{S}(\omega)$ is not shown here, but it can be found in Marcela at al. (2020).

3.4. Spectral transfer matrix method

The spectral transfer matrix method (STM) (Lee, 2000) is an analytical spectral approach of the system in the state-space form to directly obtain the transfer matrix of the structure. The spectral elements are formulated by the exact shape functions derived from the wave solutions of a structural model. The spectral element matrix can be derived from the transfer matrix spectrally formulated directly from a state vector equation of motion. From dynamic system relationship, a frequency-domain state-vector equation can be obtained as,

$$\frac{d\hat{\boldsymbol{y}}}{dx} = \boldsymbol{A}(\omega)\hat{\boldsymbol{y}} \qquad (0 \le x \le L), \tag{28}$$

where $\boldsymbol{A}(\boldsymbol{\omega})$ is the system coefficient matrix with $[\boldsymbol{2n} \times \boldsymbol{2n}]$ DOFs, and $\hat{\boldsymbol{y}}(\boldsymbol{x}) = \{\hat{\boldsymbol{d}} \;\; \hat{\boldsymbol{F}}\}^{\boldsymbol{T}}$ is the state vector with $\hat{\boldsymbol{d}}$ as the nodal displacements vector and $\hat{\boldsymbol{F}}$ the internal nodal forces vector. The general solution of Eq. (28) for a structural element of lebgth $\boldsymbol{L}$ is given by,

$$\hat{\boldsymbol{y}}(\boldsymbol{L}) = \boldsymbol{e}^{\boldsymbol{AL}}\hat{\boldsymbol{y}}(\boldsymbol{0}) = \mathbf{T}(\boldsymbol{\omega})\hat{\boldsymbol{y}}(\boldsymbol{0}), \tag{29}$$

where $\mathbf{T}(\boldsymbol{\omega}) = \boldsymbol{e}^{\boldsymbol{AL}}$ is the transfer matrix, which is a exponential matrix. If all eigenvectors of the matrix $\boldsymbol{A}$ are linearly independent, the transfer matrix can be obtained by (Shi and Mak, 2017):

$$\mathbf{T}(\boldsymbol{\omega}) = \boldsymbol{\Psi}\boldsymbol{e}^{\boldsymbol{\lambda L}}\boldsymbol{\Psi}^{-\mathbf{1}} \tag{30}$$

where $\boldsymbol{\lambda}$ is the eigenvalue diagonal matrix and $\boldsymbol{\Psi}$ is the corresponding eigenvector of matrix $\boldsymbol{A}$. Substituting $\mathbf{T}(\boldsymbol{\omega})$ in Eq. (17) Bloch wavenumbers and wave modes can be computed.

4. Numerical results

For the numerical tests, it is considered a simply supported and free-free boundary conditions and the conductor cable had the follows mechanical properties: Young's modulus of E = 74 GPa, mass density ρ = 2700 kg/m3 and structural loss factor η = 0.01. Tensile forces of T = 0.27, 2.7 and 27 kN were used. The cable geometry are: length L = 100 m and circular cross section area A = 50 mm^2.

Table 1 shows the resonance frequencies of the simply supported cable estimated by Analytical Solution (AS), SEM, and FEM with different number of elements and tensile force T = 27 kN. As expected the SEM results present the same resonance frequencies values of the AS, and FEM result converges to AS and SEM as the number of elements increases, which implies in high computational cost. In order to minimize the resonance frequency error between SEM and FEM close to zero a number of 100 elements must used in FEM discretization.

Table 1. Cable resonance frequency.

Mode	Resonance frequencies					
	Analytical	SEM	FEM 10 elem.	FEM 20 elem.	FEM 50 elem.	FEM 100 elem.
1º	0.22	0.22	0.22	0.22	0.22	0.22
2º	0.45	0.45	0.44	0.45	0.45	0.45
3º	0.67	0.67	0.65	0.67	0.67	0.67
4º	0.90	0.90	0.85	0.89	0.89	0.90
5º	1.13	1.13	1.04	1.11	1.12	1.13

The displacement responses are calculated using the FEM model with 100 elements discretization and tensile load of 0.27, 2.7 and 27 kN. Figure 5(a) shows the displacement response obtained close to the right end boundary with unitary excitation applied at the same measure point, and the tensile load applied in the cable was 0.27 kN. The SEM and FEM presented similar resonance frequencies in the whole frequency range. The displacements are close with a slight amplitude difference in the first and second resonance frequency. Figure 5(b) shows the comparison of displacement response obtained with FEM and SEM with a tensile load 2.7 kN. At low frequency band the displacement amplitude presents high differences until the frequency of 0.7 Hz, after that the results are in good agreement.

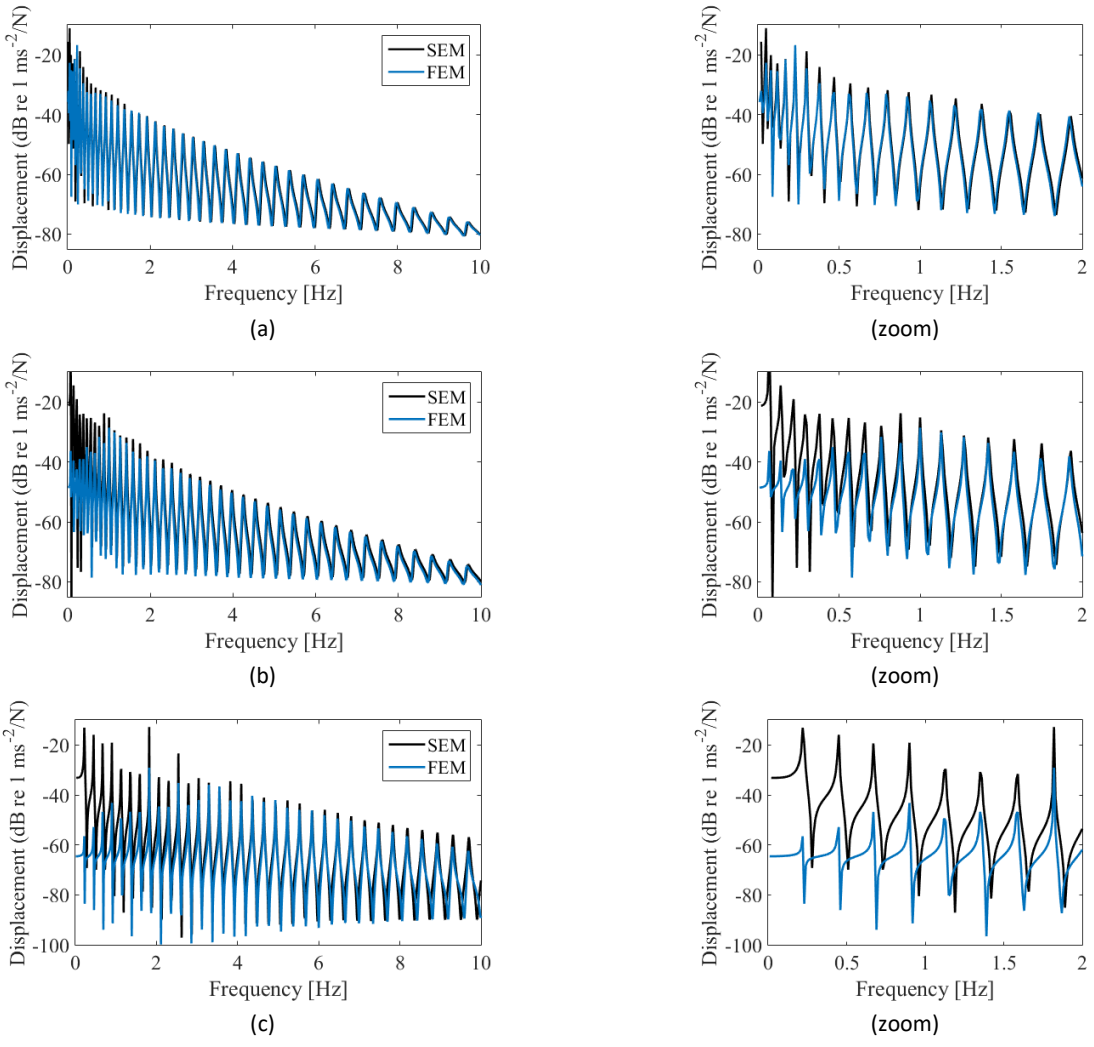

Figure 5. Cable displacement response by SEM and FEM using a tensile load: (**a**) T = 0.27 kN; (**b**)T = 2.7 kN;(**c**) T = 27 kN.

Figure 5(c) presents the displacement response for a tensile load of 27 kN. The SEM and FEM presents similar results as before where t lo frequency band the amplitudes disagree until the frequencies of 2 Hz and after that they agree. In brief as the tensile load increases, the FEM differ of SEM in displacement amplitudes for low frequency band. However, the resonance frequencies remain with good approximation in all cases and the whole range of frequency analyzed.

The next analysis evaluates the comparison among SEM with a single element, FEM with 100 elements, and WFE with 100 unit-cells (1 mm length) to calculate forced responses. The SEM, WFE and STM are used to obtain the flexural wave propagation. To simplify, it is assumed a free-free boundary condition and the same conductor cable properties and geometry of the previous study. For the WFE the cable is excited by a unit vertical harmonic force applied at the cable left end, and the response is obtained on the left and right end to further estimate the transmissibility response. For the SEM and FEM the cable is excited in the right end and response are obtained in both ends.

Figure 5(a) displayed the comparison of the transmissibility response of the cable under a tensile load of 0.27 kN calculated by SEM, FEM and WFE, where a CPU time of 4.52, 7.73, and 9.67 seconds were recorded, respectively. The computational time was obtained using a Dell micro-computer with an Intel (R) Core i7-8750H 2.20HHz processor and 8 GB RAM under the same conditions. By comparing the transmissibility responses in a frequency band of 0 to 10 Hz, the results are in good agreement for all methods.

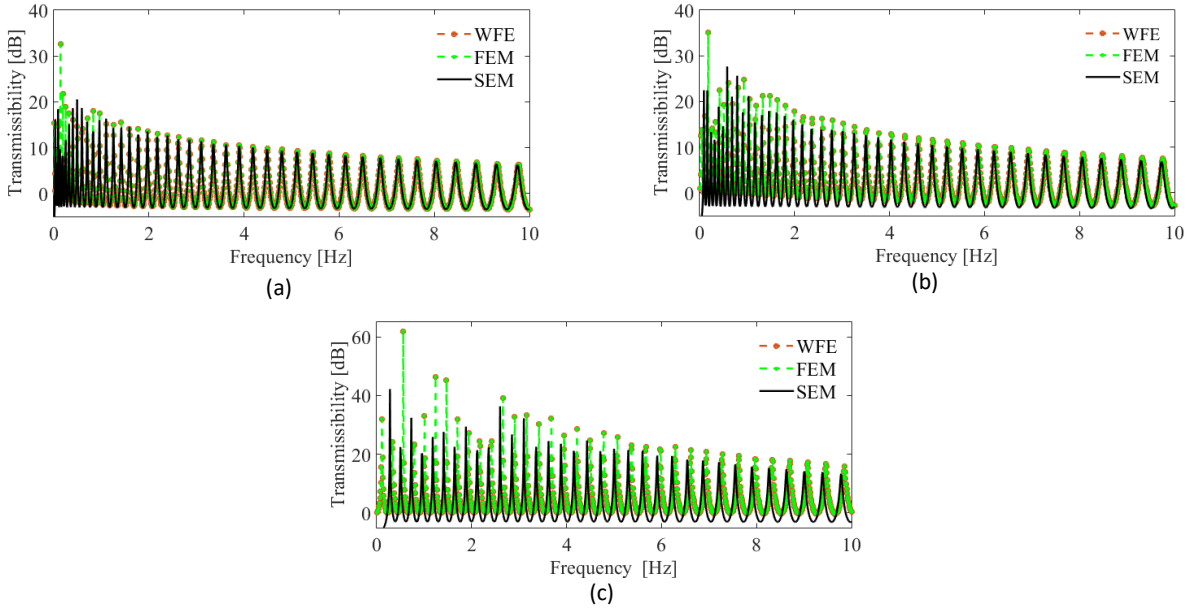

Figure 6. Cable transmissibility by SEM, FEM and WFE using a tensile load: (a) T = 0.27 kN; (b) T = 2.7 kN;(c) T = 27 kN.

Figure 6(b) shows the transmissibility response of the cable under tensile load of 2.7 kN. Transmissibility calculated by SEM, WFE and FEM presented good agreement, and computation times are 4.50, 8.64, and 10.21 seconds, respectively. Figure 5(c) shows the transmissibility response for the tensile load of 27 kN where the results by FEM and WFE are in good agreement, but differs from the SEM. SEM derives from the analytical solution of the wave equation, as a consequence, the solution is accurate and follows the analytical solution, which makes SEM response our reference among the numerical techniques. The WFE follows the FEM response because both use the same approximated solution. For a free-free boundary condition, both methods could not evaluate accurate transmissibility for a higher tensile load which did not occur for a supported boundary condition. As both techniques work with discretisation procedure, a higher number of elements in the mesh were required to properly include the tensile load effect in this continuous system. The computation time for SEM, WFE, and FEM was 4.30, 8.21, and 8.93 seconds, respectively.

For all cases, the transmissibility responses estimated with the three numerical methods presented good results with a slight difference in the resonances as the tensile load increased. SEM was the faster technique followed by WFE and FEM.

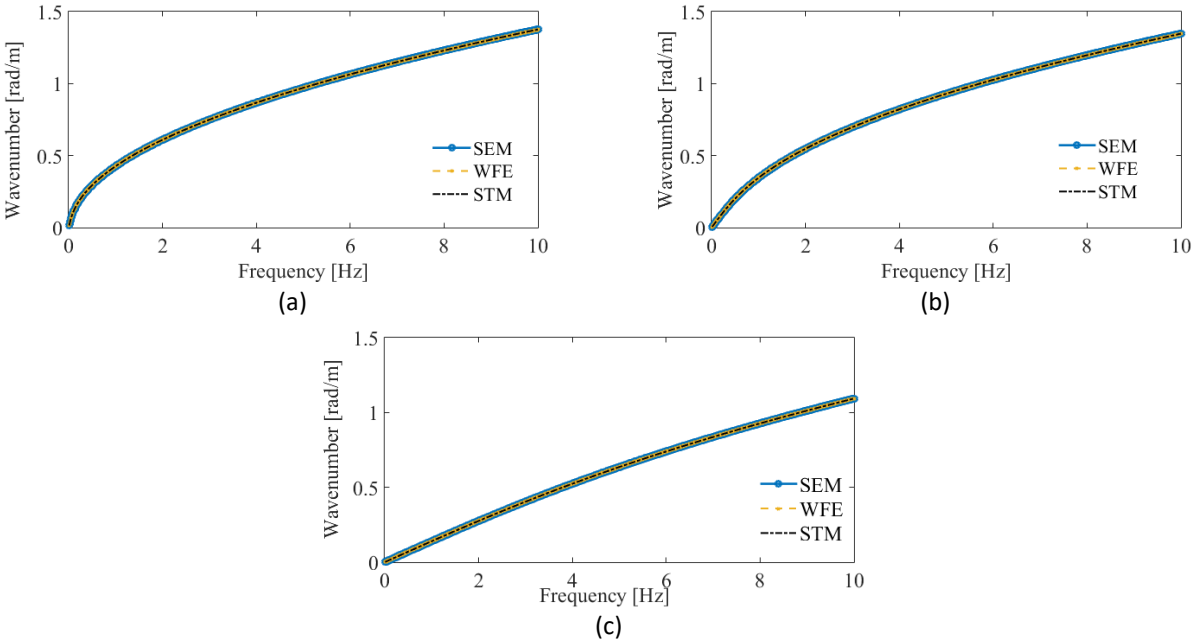

Figure 7. Cable dispersion diagram by SEM, WFE, and STM using tensile loag: (a) T = 0.27 kN; (b) T = 2.7 kN;(c) T = 27kN

The dispersion diagrams were calculated by SEM, WFE and STM with the tensile load of T = 0.27, 2.7 and 27 kN. The results are shown in Figure6(a-c), and for all methods as the tensile load increases the wave modes changed from non-dispersive for T = 27 kN to dispersive ones when T is up to 2.7 kN. Similar dispersion diagram was obtained with the methods. In practice, the wave modes type defines how the wave pack will propagate into the structure. For a non-dispersive dispersion diagram, the waves of the package travel at the same speed and group velocity, having no changes in the waveform. For the dispersive media, it leads to a wave pack spreading out and changes shape as it travels and propagating in speed. The cable media can induce both dispersion types only by changing the tensile load, as demonstrated in figure 7.

5. Conclusions

The article presents a numerical model of the overhead transmission cables through the analytical models, SEM, FEM, WFE and STM. As expected, the resonance response obtained with the SEM present the same value as the analytical solution, and the FEM results shown a better approximation in relation to SEM and the analytical solution as the number of elements increases. By comparing SEM, FEM and WFE, the transmissibility responses presented similar resonance frequencies, and the SEM presented a precise solution due to its derivation is from the analytical solution of the wave equation. WFE, on the other hand, presented the same response as FEM, since both use the same mass and stiffness matrices. The dispersion diagram is similar for all methods used in the estimation and as the tensile loads increase the wave kind change from dispersive to non-dispersive. Finally, we conclude that all numerical methods presented a good approximation to each other, with a small difference in the resonances as the tensile load increases.

References

1. B.R. Mace, D. Duhamel, M.J. Brennan, L. Hinke, Finite element prediction of wave motion in structural waveguides, Journal of the Acoustical Society of America 117 (5) (2005) 2835–2843, http://dx.doi.org/10.1121/1.1887126.
2. B. R. Mace, E. Manconi, Modelling wave propagation in two-dimensional structures using finite element analysis, Journal of Sound and Vibration, vol. 318, no. 45, (2008), pp. 884 902. doi: https://doi.org/10.1016/j.jsv.2008.04.039.

3. D. Duhamel, B. Mace,M. Brennan, Finite element analysis of the vibrations of waveguides and periodic structures, Journal of Sound and Vibration, vol. 294, no. 12, (2006), pp. 205 220. doi: https://doi.org/10.1016/j.jsv.2005.11.014.
4. Dutkiewicz, M.; Machado, M. R.Dynamic Response of Overhead Transmission Line in Turbulent Wind Flow with Application of the Spectral Element Method. IOP Conference Series: Materials Science and Engineering. , v.471, p.052031 , (2019.b)
5. Dutkiewicz, M.; Machado, M.R. Measurements in Situ and Spectral Analysis of Wind Flow Effects on Overhead Transmission Lines. Sound and Vibration. , v.53, p.161 - 175, (2019.b)
6. Dutkiewicz, M; Machado, M.R.Spectral Approach in Vibrations of Overhead Transmission Lines. IOP Conference Series: Materials Science and Engineering. , v.471, p.052029 - , (2019.a)
7. Dutkiewicz, M.; Machado, M. R. Spectral element method in the analysis of vibrations of overhead transmission line in damping environment. Structural Engineering and Mechanics, v. 71, p. 291-303, (2019.d)
8. Fu, X.; Li, H. N. Dynamic analysis of transmission tower-line system subjected to wind and rain loads. Journal of Wind Engineering and Industrial Aerodynamics, Elsevier, v. 157, p. 95–103, (2016).
9. Lee U. Vibration analysis of one-dimensional structures using the spectral transfer matrix method. Eng Struct (2000), 22:681–90. doi: https://doi.org/ 10.1016/s0141-0296
10. Li, X. et al. Probabilistic capacity assessment of single circuit transmission tower-line system subjected to strong winds. Engineering Structures, Elsevier, v. 175, n. July, p. 517–530, 2018. ISSN 18737323
11. Machado, M.R.; Dutkiewicz, M.; Matt, C.F.T.; Castello, D.A. Spectral model and experimental validation of hysteretic and aerodynamic damping in dynamic analysis of overhead transmission conductor. Mechanical Systems and Signal Processing. v.136, p.106483 - , (2020). doi: https://doi.org/10.1016/j.ymssp.2019.106483
12. Mencik, J.-M., Approche numerique pour la propagation multi-modale guidee, Université Francois Rabelais de Tours (2008).
13. Rao, S. S., Mechanical Vibrations, 6th Ed., (2018), p.778.
14. Xiao,Y., Wen, J. , Wen, X.Longitudinal wave band gaps in metamaterial-based elastic rods containing multi-degree-of-freedom resonators, New Journal of Physics, vol. 14, no. 3, (2012), p. 033042.
15. S. Bischoff, C. Schaal, L. Gaul, Efficient wave scattering analysis for damaged cylindrical waveguides, Journalof Sound and Vibration 333 (18) (2014) 4203–4213.
16. C. Schaal, S. Bischoff, L. Gaul, Analysis of wave propagation in periodic 3d waveguides, Mech. Syst. Signal Process. 40 (2) (2013) 691–700.
17. O.C. Zienkiewicz, R.L. Taylor, The Finite Element Method, Butterworth-Heinemann, 2000.
18. U. Lee, Spectral Element Method in Structural Dynamics, BInha University Press, 2004.
19. J.F. Doyle, Wave Propagation in Structures, Springer Verlag, New York, 1997.
20. J.-M. Mencik and M.N. Ichchou, Multi-mode propagation and diffusion in structures through finite elements, European Journal of Mechanics - A/Solids, 24(5), (2005), 877-898, doi: http://dx.doi.org/10.1016/j.euromechsol.2005.05.004 .
21. P. B. Silva, J.-M. Mencik, J. R. Arruda, On the Forced Harmonic Response of Coupled Systems via a WFE-Based Super Element Approach, Proceedings of ISMA 2014, (2014), 1–13.
22. W. Zhong, F. Williams, On the direct solution of wave propagation for repetitive structures, Journal of Sound and Vibration, 181(3), (1995), 485–501, doi:http://dx.doi.org/10.1006/jsvi.1995.0153.
23. Shi X, Mak C-M. Sound attenuation of a periodic array of micro-perforated tube mufflers. Applied Acoustics (2017);115, doi: http://dx.doi.org/10.1016/j.apacoust.2016.08.017
24. M. R. Machado, M. Dutkiewicz, C. F. T. Matt, D. A. Castello, Spectral model and experimental validation of hysteretic and aerodynamic damping in dynamic analysis of overhead transmission conductor, Mechanical Systems and Signal Processing, 136, (2020), 106483, doi: https://doi.org/10.1016/j.ymssp.2019.106483
25. E.D. Nobrega, F. Gautier, A. Pelat, J. M. C. Dos Santos, Vibration band gaps for elastic metamaterial rods using wave finite element method, Mechanical Systems and Signal Processing, 79, (2016), 192–202. doi:http://dx.doi.org/10.1016/j.ymssp.2016.02.059